Boundary-Layer Meteorol (2008) 127:37–56
DOI 10.1007/s10546-007-9252-z

ORIGINAL PAPER

Identifying Nonstationarity in Turbulence Series

Edgar L Andreas · Cathleen A. Geiger · George Treviño · Kerry J. Claffey

Received: 23 May 2007 / Accepted: 26 November 2007 / Published online: 20 December 2007
© Springer Science+Business Media B.V. 2007

Abstract Because of rapid forcing by varying cloud and sky conditions, turbulence time series collected in the atmospheric surface layer over land may often be nonstationary. The meteorological community, however, has no consensus definition of what nonstationarity is and, thus, no consensus method for how to identify it. This study, therefore, adopts definitions for rst-order and second-order stationarity taken from the time series analysis literature and implements new analysis techniques and probabilistic tests to quantify rst-order and second-order nonstationarity. First-order nonstationarity manifests as a change in the series mean; second-order nonstationarity, as a change in the variance. The analysis identi es nonstationarity in surface-level turbulent temperature and water vapour series collected during two sample days with solar forcing in uenced by cirrus and cirrostratus clouds, but that nonstationarity is not as severe as expected despite the rapid thermal forcing by these clouds. On the other hand, even with negligible cloud forcing, both sample days exhibited severe nonstationarity at night.

Keywords Atmospheric surface layer· Cloud forcing· Integral scale Nonstationarity· Time-dependent memory method (TDM method)· Time series analysis

E. L Andreas (✉)
North West Research Associates, Inc. (Seattle Division), 25 Eagle Ridge, Lebanon, NH 03766-1900, USA
e-mail: eandreas@nwra.com

C. A. Geiger
Department of Geography, Center for Climatic Research, University of Delaware, Newark, DE, USA

G. Treviño
CHIRES, Inc., San Antonio, TX, USA

K. J. Claffey
U.S. Army Cold Regions Research and Engineering Laboratory, Hanover, NH, USA

1 Introduction

The atmospheric boundary layer is inherently nonstationary. The sun rises and sets. Fair-weather clouds pass overhead and periodically shade the surface. Thicker, more extensive, cloud layers provide even more shading during daylight hours and act as a blanket against radiative cooling at night. Moreover, the transition in sky conditions as these cloud layers develop or dissipate affects the surface temperature just as do fair-weather clouds and sunrise and sunset transitions.

The lower atmosphere responds almost immediately (order of tens of seconds) to this rapid surface forcing because the forcing manifests first as a change in surface temperature. The surface temperature, in turn, feeds into the sensible and latent heat fluxes, which affect the near-surface atmospheric temperature and humidity profiles in short order. A change in the sensible heat flux also alters the near-surface atmospheric stratification and, thus, quickly influences the wind speed profile.

Monin–Obukhov similarity theory, which organizes our understanding of the atmospheric boundary layer—especially the atmospheric surface layer—relies on two assumptions that seem at odds with this depiction of the atmospheric boundary layer: (1) that the atmosphere is statistically stationary, and (2) that the surface is horizontally homogeneous. In fact, in some cases, the nonstationarity and the horizontal inhomogeneity go hand-in-hand, even when the surface appears visually homogeneous. For example, anyone who has flown over the U.S. Great Plains (or similar terrain on other continents) on a late-summer day featuring fair-weather cumulus may have noticed the light and dark patches that the cloud shadows create on the uniformly brown surface. Surface temperatures in the cloud shadows can be 5–10°C lower than in full sunlight. Hence, a meteorological tower fixed on the surface would experience the nonstationarity of the passing clouds and also the horizontal inhomogeneity caused by the resulting spatial variability in surface temperature (cf. Roth and Oke 1995).

While Kukharets and Tsvang (1998) previously documented the variability in surface temperature over visually homogeneous terrain, they made their measurements under clear skies and inferred that fluctuations in the wind caused the temperature variability that was observed. Roth and Oke (1995) hypothesized that broken clouds lead to spatial variability in surface temperature but reported no observations to support this notion. Stoll and Stoll et al. (2002) studied the effects of cloud shadows on the structure of the convective boundary layer with a radiative transfer model and large-eddy simulation. They did not study the surface response to changes in cloud forcing but simply assumed that the surface responds immediately. They offered no data to support this assumption or their model results.

Because clouds are ubiquitous, we speculate that many of the measurements of the Monin–Obukhov similarity functions that have been reported were collected in nonstationary conditions. Such violations of the premises on which Monin–Obukhov similarity rests may explain some of the scatter that still exists in these "universal" similarity functions despite almost 50 years of measurements to quantify them (e.g., Högström 1996; Andreas et al. 1998; Johansson et al. 2001; Andreas 2002; Klipp and Mahrt 2004).

Still, the measured Monin–Obukhov similarity functions are not wildly scattered, just perplexingly scattered. Perhaps the need for stationary conditions is not a strong constraint on Monin–Obukhov similarity theory. Our premise here, though, is that we know so little about how to handle or even to judge nonstationarity that we cannot make progress in determining its consequences without a better way to characterize it.

Foken and Wichura (1996), Vickers and Mahrt (1997), Mahrt (1998), and Andreas et al. (2003), among others, have described methods for identifying nonstationarity in turbulence series from the atmospheric boundary layer. But these authors alone describe at least five

methods for identifying nonstationarity: for example, comparing statistics from short series to statistics from longer series, computing trends, counting zero crossings, and using information on the probability density function. That is, the community has reached no consensus on how to identify nonstationary.

Here we present yet another method for identifying nonstationarity, but our method has three advantages: it has a theoretical basis, it relies on accepted definitions of what constitutes nonstationarity, and it assigns a probability as to whether any nonstationary period it identi es is truly nonstationary.

Averaging a nonstationary time series is a fundamental problem because, by definition, the resulting statistics depend on when you begin to average and how long you average. We average using Treviño and Andreas (2000) time-dependent memory method (TDM method), which was formulated especially to extract the mean and turbulent uctuations from a nonstationary series. We then invoke Priestley (1981) definitions of rst-order and second-order nonstationarity and use standard statistical functions to test for rst-order and second-order nonstationarity. These functions also let us assign significance levels to these tests.

The data we use in these analyses come from a dedicated experiment during which we deployed a suite of radiation instruments to characterize forcing by sun, sky, and clouds and the surface's response to this forcing. We combine these radiation measurements with turbulence measurements to document the concomitant near-surface atmospheric response to the radiative forcing. Our analysis reveals nonstationarity in the near-surface air temperature and humidity associated with rapid changes in sky condition. Andreas et al. (2006, 2007) have reported some of our preliminary results.

2 Measurements

The data we use in our analysis come from a 2-week experiment conducted in a 15-acre eld in Lebanon, New Hampshire, in April 2005. The eld had been mowed the previous autumn and was, thus, covered in grass stubble and clippings a few tens of mm thick. When the experiment began, the grass was dormant and the ground was cold, with the soil still frozen a few tens of mm below a thawed surface layer. The grass greened up noticeably by the end of the experiment, however, but was still short.

We used Eppley hemispherical, broadband longwave (model PIR) and shortwave (model PSP) radiometers to measure incoming and outgoing longwave and shortwave radiation. We also used Heitronics infrared thermometers to measure the sky (model KT 19.85II, wavelength 9.6–11.5 μm) and surface (model KT 19.81II, wavelength 8–14 μm) temperatures. These are narrow-beam radiometers, with a 2.5° eld of view. Our last radiation instrument was a Thermoscan model S60 digital infrared camera from FLIR Systems, operating in the 7.5–13 μm wavelength band with 76,800 pixels in its eld of view.

We sampled the Eppley radiometers and the Heitronics thermometers at 1 Hz and will concentrate on this rapidly sampled data in our analysis. We obtained an image from the infrared camera once a minute and averaged over its entire eld of view to obtain the average surface temperatures.

Later, we show temperatures obtained by converting the longwave radiation, Q_L, from both the Eppley up-looking and down-looking instruments to a blackbody temperature using

$$T_{BB} = (Q_L/\sigma)^{0.25}. \quad (1)$$

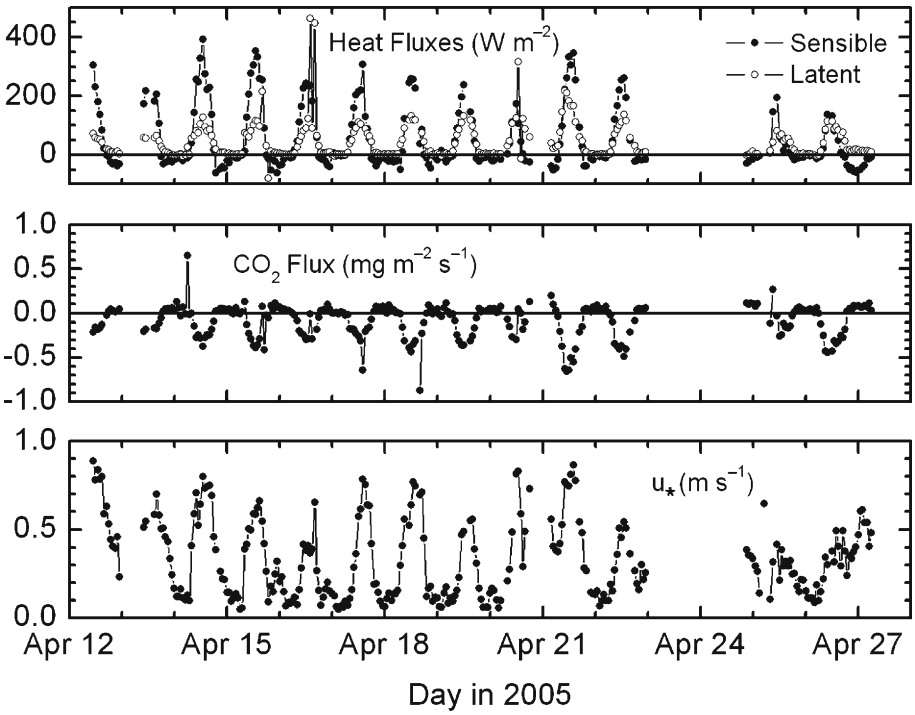

Fig. 1 Hourly eddy-correlation measurements of the sensible and latent heat fluxes, the flux of carbon dioxide, and the friction velocity (u_*) for the duration of our experiment. Gaps were periods of rain that ruined the data from the sonic anemometer/thermometer. Positive heat and CO_2 fluxes are upward

This gives T_{BB} in kelvins when Q_L is in W m^{-2}, where σ (= 5.670400 × 10^{-8} W m^{-2} K^{-4}) is the Stefan–Boltzmann constant. The Heitronics thermometers and the infrared camera also measured the blackbody temperature because we set their adjustable emissivity values to one.

Near these radiation instruments, we had a "turbulence" tower with a three-axis, K-type sonic anemometer/thermometer from Applied Technologies Inc. (Kaimal et al. 1990; Kaimal and Gaynor 1991; Kaimal and Finnigan 1994, p. 218f.) mounted 3.6 m above the surface. Placed just below the sonic (Christensen et al. 1997) was a Li-Cor 7500 fast-responding water vapour and carbon dioxide sensor. We sampled all of these instruments at 10 Hz, and later show time series of these turbulence signals subsampled at 1 Hz simply for convenience. We do use the 10-Hz data, though, for calculating statistics.

Finally, we documented sky conditions with periodic photographs from an all-sky camera (Nikon Coolpix 4500 with a Nikon fisheye converter lens).

To place the analyses that we will describe in context, we show in Fig. 1 hourly averages of the turbulent fluxes for the duration of our experiment. To obtain these fluxes, we did standard turbulence processing. That is, we rotated the measured wind components into a frame that was horizontal and aligned with the mean wind. We detrended each hourly time series, if necessary, using the method described in Andreas and Treviño (1997). Lastly, we applied the Webb correction (Webb et al. 1980; Fuehrer and Friehe 2002) to the water vapour and carbon dioxide fluxes.

The friction velocity (u_*) plotted in Fig. 1 shows that wind speeds were typically moderate during the day and low at night. Both the sensible and latent heat fluxes respond to this

wind forcing and surface heating by the sun during the day. At night, the sensible heat flux becomes downward, and the latent heat flux is near zero. Hence, during most afternoons, the atmospheric surface layer was unstably stratified; at night, it was weakly stable.

The flux of carbon dioxide in Fig. 1 is the mirror image of the heat fluxes. Photosynthesis produces a downwards carbon dioxide flux during daylight, and respiration by the plants and micro-organisms in the soil produces a small net upward flux of carbon dioxide during the night.

These CO_2 fluxes are similar to those that others have measured by eddy correlation over vegetative surfaces (e.g., Pattey et al. 2002; Gao et al. 2003; Jacobs et al. 2003; Siqueira et al. 2003). If anything, the magnitudes of our fluxes may be somewhat smaller because our experiment occurred early in the growing season (e.g., Jacobs et al. 2003). Our nighttime fluxes, in particular, were generally smaller than those reported by Pattey et al. (2002), probably because nighttime temperatures—typically around 0 °C—were 15–20 °C lower than the temperatures during their measurements.

3 Quantifying the Nonstationarity

One of the central issues in atmospheric turbulence research is deciding how long to average a turbulence time series to obtain meaningful estimates of the mean, the variance, and the turbulent fluxes (e.g., Lumley and Panofsky 1964, p. 35ff.; Wyngaard 1973; Sreenivasan et al. 1978; Andreas 1988; Lenschow et al. 1994). Most attempts to answer this question implicitly assume that the turbulence time series is stationary; but in light of the number of time scales represented in the forcing (see Sect. 2), we believe that an analysis based on a broader assumption that includes nonstationarity may be more realistic.

Turbulence analyses typically begin with an instantaneous measurement of some variable $\tilde{x}$ (e.g., the longitudinal wind component). The purpose of averaging is to separate this instantaneous value into mean (X) and turbulence (x) components such that

$$\tilde{x} = X + x. \tag{2}$$

When a series is nonstationary, however, the mean of $\tilde{x}$ may not be approximately constant over typical hour-long averaging periods; X is thus ill-defined. The average amplitude of x may also vary. We show both manifestations of nonstationarity in our later figures.

Treviño and Andreas (2000), however, developed a rational procedure to separate the mean and the fluctuations, as required in (2), in a turbulence series that is assumed to be nonstationary. The method applies equally well, though, to stationary series. Treviño and Andreas call their technique the time-dependent memory method (TDM method; U.S. Patent No. 6,442,506) because it finds two time scales for averaging. One scale, called ΔT, defines an averaging window over which to compute the mean (X), and, in turn, to separate the turbulent part (i.e., x). Finding ΔT requires that we specify the measurement accuracy, r, and invoke the constraint that we cannot know a property to better precision than our measurement accuracy.

We later apply the TDM method to two of the measured turbulence variables: temperature from the sonic thermometer and water vapour density from the Li-Cor 7500. As the accuracy for the temperature, we used 0.01 °C. As the accuracy for the water vapour density, we used 1% of the daily average in water vapour density. Andreas and Treviño (1997) also used sensor accuracy as a criterion for detrending a turbulence series.

A second time scale in the TDM method, the "memory," derives as the decorrelation time implied by the autocorrelation function of the turbulent part. We obtain L as the

integral of the autocorrelation function r out to the lag that produces the maximum for the integral (see Treviño and Andreas 2000). Treviño and Andreas (2000) then take 10 I_r as the averaging window over which to compute the variance $\sigma^2 = \overline{x^2}$, where the overbar indicates a time average. Using 10 I_r as the window for computing σ^2 provides an adequate number of independent samples. Usually I_r is computed to be less than 1 ΔT; if it is not, we set the averaging time for computing variance to ΔT. Treviño and Andreas (2000) elaborate further on the advantages of an averaging scheme that uses distinct windows for finding X and σ^2 compared to traditional block averaging.

Once we have used the time-dependent memory method to choose proper averaging times, we can compute the mean and variance at regular intervals through that series and can test whether the series is stationary or nonstationary. Priestley (1981, p. 104ff.) describes the concept of a process that is stationary at order n. If a process is order-1 (first-order) stationary, its mean does not change with time. If a process is order-2 (second-order) stationary, its variance does not change with time. Our testing for order-1 and order-2 stationarity is akin to using the probability density function to test for stationarity (e.g., Kennel 1997).

Under the hypothesis that the mean is constant—that is, that a series is first-order stationary—the statistic

$$t = \frac{X_\mathrm{i} - X_{\mathrm{i}+1}}{\left[\frac{\sigma_\mathrm{i}^2}{n_{\mathrm{i}+1}} + \frac{\sigma_{\mathrm{i}+1}^2}{n_\mathrm{i}}\right]^{1/2}} \left[\frac{n_\mathrm{i} + n_{\mathrm{i}+1} - 2}{n_\mathrm{i} + n_{\mathrm{i}+1}}\right]^{1/2} \tag{3}$$

has a Student's t distribution with zero mean, variance 1, and $n_\mathrm{i} + n_{\mathrm{i}+1} - 2$ degrees of freedom. Here X_i and $X_{\mathrm{i}+1}$ and σ_i^2 and $\sigma_{\mathrm{i}+1}^2$ are the means and variances of adjacent intervals in a turbulence time series, computed using the TDM method, and n_i and $n_{\mathrm{i}+1}$ are the number of independent samples used to compute the variances. By computing t, we can test for first-order nonstationarity.

If the x values derive from a normal distribution, the resulting sample variances can be represented with a χ^2 distribution; then, the statistic

$$F = \frac{n_\mathrm{i}\sigma_\mathrm{i}^2\,(n_{\mathrm{i}+1} - 1)}{n_{\mathrm{i}+1}\sigma_{\mathrm{i}+1}^2\,(n_\mathrm{i} - 1)} \tag{4}$$

has an F distribution with $n_\mathrm{i} - 1$ and $n_{n+1} - 1$ degrees of freedom (e.g., Brunk 1965, p. 260). Because (4) involves only variances, we can test for second-order nonstationarity by computing F for adjacent intervals.

We worry, though, that the F statistic is known to be sensitive to deviations from a normal distribution (Wilks 2006, p. 165f.), and we might expect such deviations in a series that is assumed a priori to be nonstationary. The TDM method, however, tends to identify locally quasi-stationary segments in nonstationary series. Hence, we expect variances in (4), which we compute using the TDM method, to be well enough behaved to make our calculations of F meaningful.

The TDM method requires separating the instantaneous turbulence signal, $\widetilde{x}(s)$, into mean, $X(s)$, and turbulence part, $x(s)$, at *every* timestep s. We computed the memory I_r and the variance σ^2, however, only at 30-s intervals. In other words, because nearby means and variances are not necessarily independent, the means (X_i and $X_{\mathrm{i}+1}$) and variances (σ_i^2 and $\sigma_{\mathrm{i}+1}^2$) that we use for the comparisons in (3) and (4) are those separated by 30-s intervals to ensure independence.

Briefly, we obtained this 30-s spacing by estimating a representative integral scale for our dataset. By integral scale here, we invoke Tennekes and Lumley (1972, p. 211) defini-

tion that $\Im$ is the time interval over which a signal is correlated with itself. As an estimate for $\Im$ in the neutrally strati ed atmospheric surface layer, Wyngaard (1973) suggests $\Im \sim z/U$, where z is the measurement height and U is the mean wind speed. Greenivasan et al. (1978) build on Wyngaard's analysis and, from high-frequency time series of temperature, humidity, and velocity components, deduce

$$\Im = \frac{4z}{U}. \tag{5}$$

From (5), we estimate the typical integral scale in our data to be 3–7 s. That is, for our data, z was 3.6 m for the sonic and about 3.2 m for the Li-Cor 7500. Wind speeds during our experiment were generally 2–5 m s^{-1}; therefore, $\Im$ typically ranges from 3 to 7 s. Consequently, we can be relatively con dent that means and variances separated by 30 s are independent, as required in (3) and (4).

The time-dependent memory method uses L as the averaging window for variance. Therefore, each variance estimate in (3) and (4) derives from 10 independent samples since L is approximately the instantaneous decorrelation time of the series. Hence, n_i and n_{i+1} are both 10 in (3) and (4). Consequently, the t distribution in (3) has 18 degrees of freedom. Then, if $|t|$ is larger than 2.878, the series is rst-order nonstationary at the 1% significance level.

Also, because n_i and n_{i+1} are the same, the F statistic in (4) reduces to $\sigma_i^2/\sigma_{i+1}^2$, and both degrees of freedom for the F distribution are 9. Therefore, the 99% con dence interval for F in (4) is $[0.153, 6.54]$. F values outside this interval indicate that a time series is second-order nonstationary at the 1% significance level.

The Appendix presents examples of distributions for the averaging window L and the memory L that we computed using the TDM method during the course of our analysis.

4 Results

Here we consider just 2 days from the experiment to demonstrate the various types of rapid forcing and to investigate nonstationarity.

Figure 2 shows time series from 26 April 2005 of incoming shortwave radiation, sky temperature from the up-looking infrared thermometer, surface temperature inferred from the down-looking Eppley longwave radiometer, and air temperature from the sonic thermometer. On a clear day, the shortwave signal would be very smooth, with a peak near 1,000 W m^{-2} around noon (Andreas et al. 2006). On 26 April, though, thin cirrus before noon and cirrus and cirrostratus after noon blocked the sun to varying degrees. The sky temperature reiterates the presence and effects of these clouds. A warming sky indicates increasing clouds, while a cooling sky signals dissipating clouds. Between midnight and 0400 h, in fact, the sky and surface temperatures were nearly the same: clouds were so thick that the surface and the clouds were nearly in radiative equilibrium. Realize, too, that the surface and sky temperatures in Fig. 2 have different sensitivities to the clouds because we measured surface temperature here with the hemispherical Eppley radiometer but sky temperature with the narrow-beam Heitronics thermometer.

The forcing by these clouds and, especially, the change in forcing, is almost immediately evident (within tens of seconds) in the surface temperature and in the air temperature in Fig. 2. For example, under the thick clouds between midnight and 0400 h, the air temperature shows very small turbulent uctuations. But when these clouds begin clearing, the surface temperature falls by about 6°C, and the air temperature likewise decreases 1–2°C. Moreover,

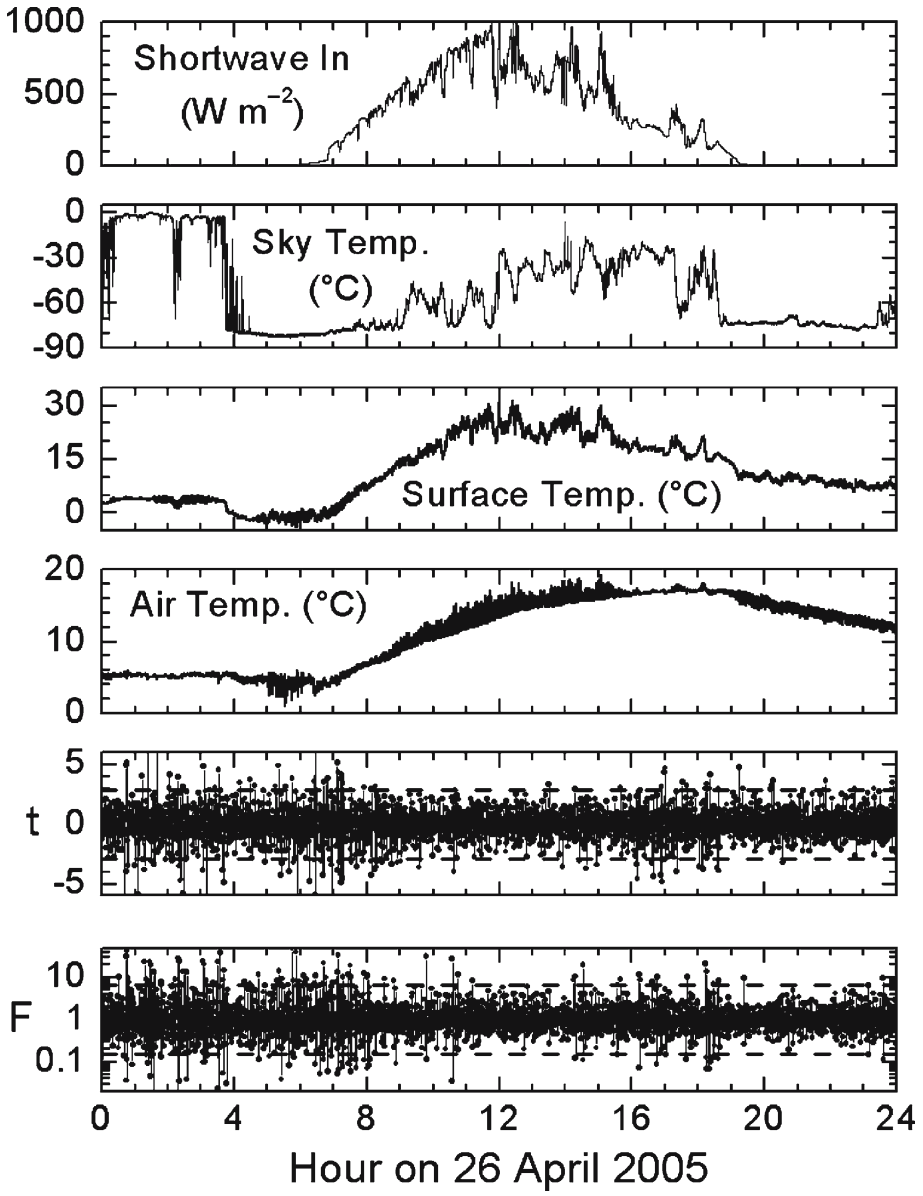

Fig. 2 Time series for 26 April 2005 of incoming shortwave radiation, sky temperature from the up-looking infrared thermometer, blackbody surface temperature from the down-looking Eppley radiometer, and air temperature from the sonic thermometer. All of these traces are 1-Hz data. The lower two panels are statistics computed every 30 s from (3) and (4) from the raw 10-Hz temperature data; horizontal dashed lines are 99% con dence limits

the air temperature shows large uctuations, evidence of downward sensible heat transfer to offset the radiative surface cooling.

During the day, one can follow ripples in the incoming shortwave radiation and sky temperature in Fig. 2 through the surface temperature and the air temperature. The spiky shortwave

trace implies that the cloud forcing can change quite rapidly; the surface and air temperatures respond almost immediately to this forcing.

Just one example of this daytime forcing in Fig. 2 is the persistent cloud from about 1500 to 1700 h. As soon as evidence of the cloud appears in the shortwave and sky traces in the gure, the surface temperature begins falling from a local maximum near 1500 h and falls almost 15°C while the cloud persists. The air temperature responds almost immediately, falling about 4°C, and the turbulent uctuations decrease to nighttime levels.

The lower two panels in Fig. 2 show time series of the t and F statistics computed from the 10-Hz temperature data. We did not detrend these data a. The F plots both contain 2,879 points. Since we are testing t and F at the 1% significance level, only about 29 points should randomly fall outside the 99% con dence intervals in each plot if the temperature series were both rst-order and second-order stationary. But many more than 29 points exceed the 99% con dence limits in both plots (137 in t, and 150 in F). That is, our analysis nds evidence of nonstationarity in the day-long temperature series.

An obvious feature of the t and F traces in Fig. 2 is that the rst 8 h of the day show many more excursions of t and F outside their respective 99% con dence limits than during the rest of the day. These statistics thus con rm a well-known observation: conditions at night are often nonstationary. But the t and F statistics also highlight periods of nonstationarity during daylight hours that evidently result from cloud forcing. For example, the cloud between 1500 and 1700 h affected air temperature enough to produce clusters of excursions beyond the 99% con dence limits in both t and F during this period.

Figure 3 shows several day-long time series from 22 April 2005. This day featured clear skies from midnight until 0900 h, as evidenced by our up-looking infrared thermometer ("Sky Temp.") seeing sky temperatures lower than its minimum instrumental range. Thin cirrus clouds, many from spreading contrails, then began forming. Next, thicker cirrostratus developed at about 1530 h and intermittently blocked and revealed the sun until about 1800 h. Finally, thicker clouds developed after sunset, as evidenced by the sky temperature.

Again, the forcing by clouds ripples quickly through the surface and air temperatures in Fig. 3. The clearest example is for the sequence between 1530 and 1800 h, which was under the in uence of cirrostratus clouds with four main clearing episodes. These four clearing events lasted only 10–15 min each (Fig. 4), yet the two surface temperatures and the air temperature all reveal nearly instantaneous warming coincident with these thinning or clearing events and significant cooling when the clouds encroach between them. The water vapour trace also shows up-going spikes that correspond with these clearing events.

Figure 5 shows the t and F statistics every 30 s for the temperature and water vapour signals depicted in Fig. 3. As with Fig. 2, we see in Fig. 5 many more excursions for t and F outside their respective 99% con dence bands between midnight and 0800 h than later in the day.

On this day, the F statistic, which quanti es changes in variance and, thus, second-order nonstationarity, seems to be a better indicator of cloud forcing than is the t statistic. For example, the F statistic for both air temperature and water vapour density responds with excursions outside the 99% con dence band when clouds encroach at about 1530 h. The corresponding t statistic here, which quanti es a change in the mean and, thus, rst-order nonstationarity, increases a small amount in magnitude but remains within the 99% con dence band at the start of the episode.

Lastly, we wish to look more closely at the midnight-to-0800-h period for 22 April and demonstrate that the t and F statistics have implications for the dynamics that govern the nonstationarity. Figures 6 and 7 combine the temperature and water vapour traces, respectively, from Fig. 3 with the t and F statistics from Fig. 5 for midnight to 0800 h on 22 April. These

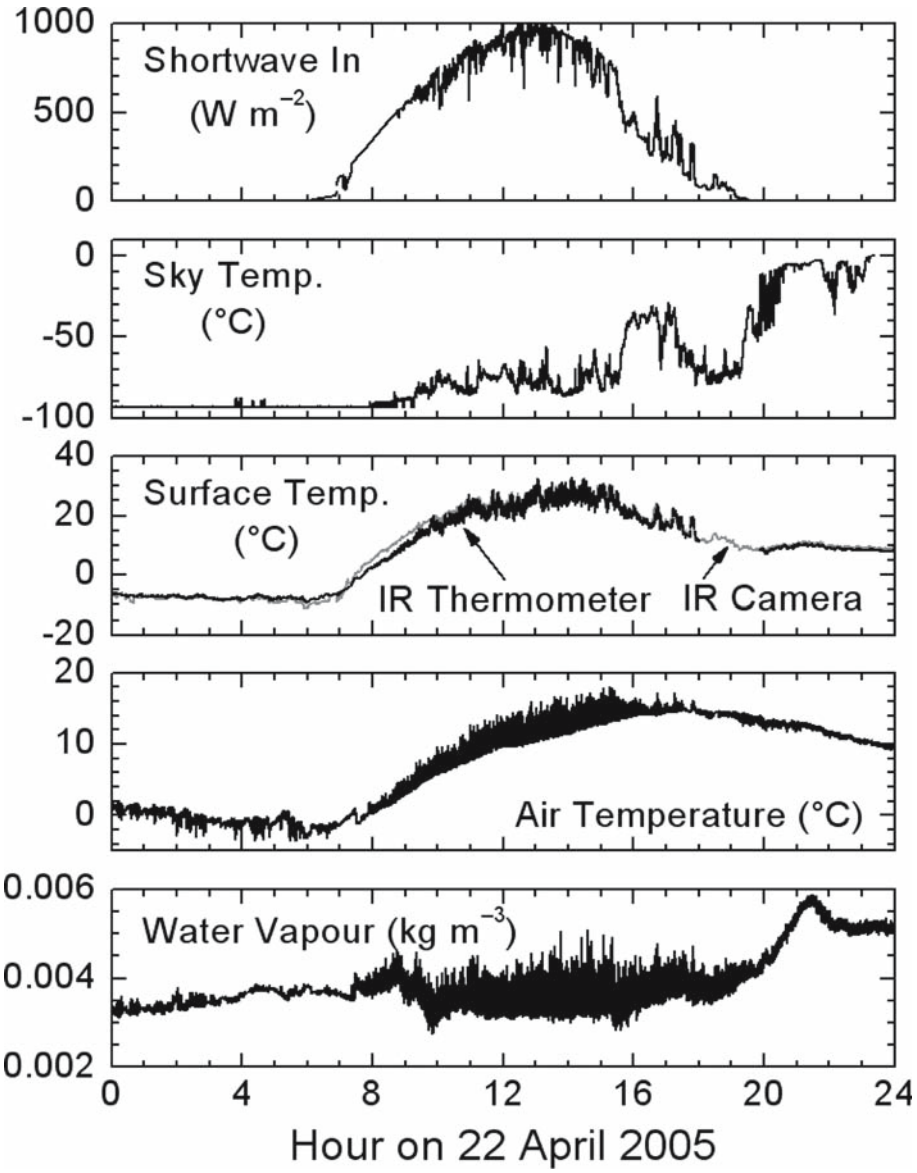

Fig. 3 Time series for 22 April 2005 of incoming shortwave radiation, sky temperature from the up-looking infrared thermometer, surface temperature measured by both the infrared camera and the down-looking infrared thermometer, air temperature measured by the sonic, and water vapour density measured by the Li-Cor 7500. All traces are 1-Hz data except the infrared camera, which sampled once a minute

expanded plots make it easier to demonstrate the behaviour in the time series of the physical variable that produces a large response in F. For example, a high peak or deep valley in the time series usually correlates with or F excursions outside the 99% con dence bands. Likewise, any quiet period in the turbulence that is followed by a relatively noisy period, or vice versa, correlates with excursions in F. The deep, steep valley in air temperature (Fig. 5) at about 0600 h, for instance, is an event that produces responses in both F. The rapid

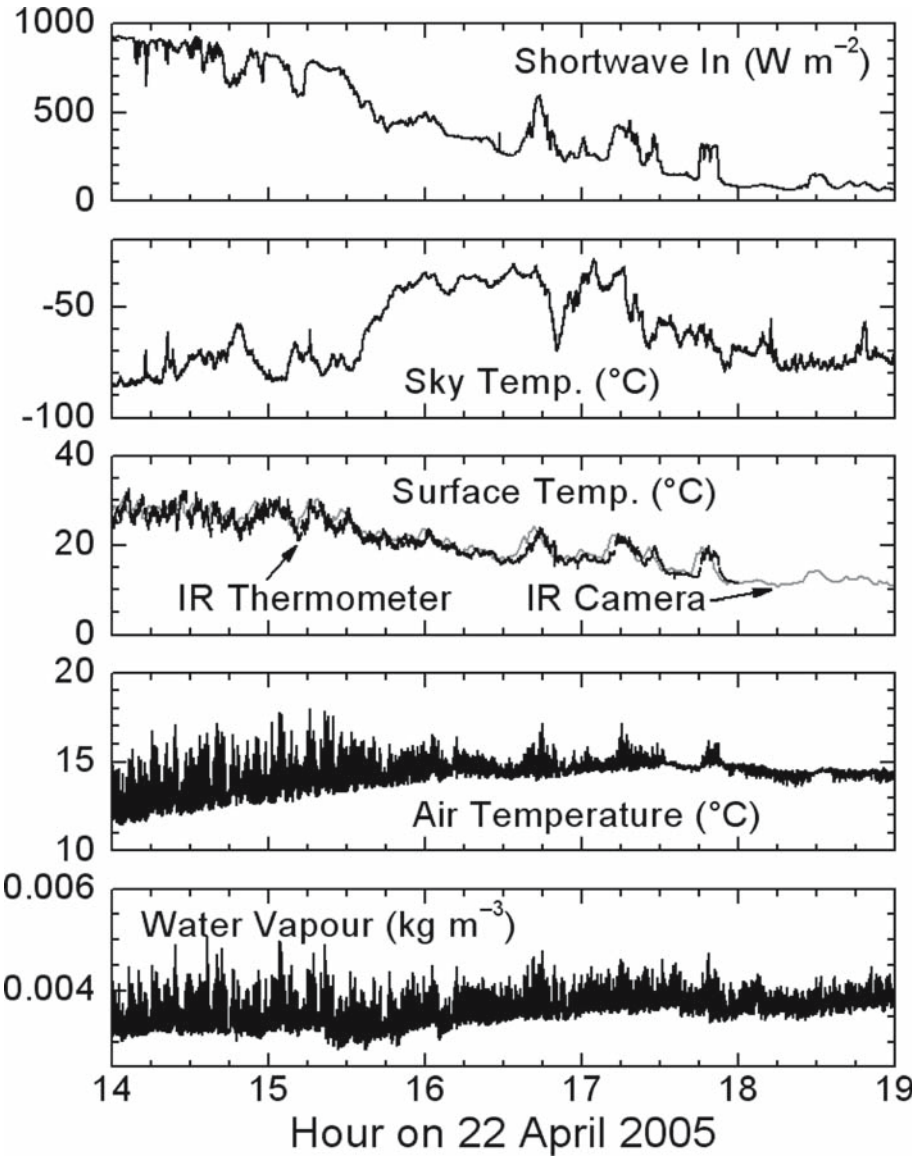

Fig. 4 As in Fig. 3, except this shows only 1400–1900 h on 22 April 2005 and focuses on the cloudy and clearing events described in the text. The "IR Camera" trace in the middle panel suggests that the clock on the infrared camera was running about 160 s fast

climb but decreasing variability in water vapour density (Fig. 7) for 0330 to 0430 h is another event producing responses in both σ and F.

Figures 8 and 9, respectively, show alternative presentations of these σ and F statistics for temperature and water vapour density. Here we take the same information as in Figs. 6 and 7 but show F versus σ. These plots more clearly show how often the series are strictly

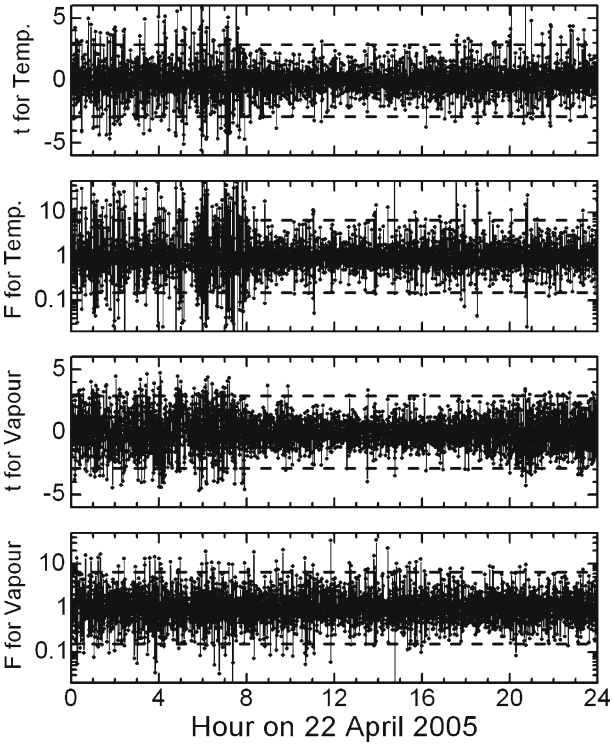

Fig. 5 The t and F statistics every 30 s computed using (3) and (4) and the raw 10-Hz data for the air temperature and water vapour series depicted in Fig. 3. The dashed lines are 99% con dence limits

stationary, rst-order but not second-order nonstationary, second-order but not rst-order nonstationary, and both rst-order and second-order nonstationary.

In the t and F scatter plot for air temperature (Fig. 8), 111 of 959 samples show rst-order nonstationarity. That is, these samples lie in sectors I–IV and b and d. Likewise, 179 of 959 samples show second-order nonstationarity. These samples lie in sectors I–IV and a and c. Since we are testing for rst-order and second-order nonstationarity at the 1% significance level, we would expect only 10 t and 10 F values (i.e., 1% of 959 samples) to randomly fall outside the central box in Fig. 8 if the data were truly stationary. We can therefore readily conclude that the air temperature data for 0000 to 0800 h on 22 April were nonstationary at either rst order or second order.

A more restrictive test might be to identify the data as nonstationary only if they exhibit rst-order and second-order nonstationarity simultaneously. In other words, only samples that fall in sectors I–IV would be indicators of a nonstationary series. Still, however, in Fig. 8, 72 samples, 7.5% of the available data, fall in these sectors. Thus, even with this narrower definition of nonstationarity, the temperature signal in Fig. 6 would still be judged nonstationary.

Figure 8 also reveals information on the dynamics of the nonstationarity. Most of the samples that display both rst-order and second-order nonstationarity fall in sector IV. Here t is negative, and F is greater than one. From our definitions of t and F [see (3) and (4)], t is negative when the mean increases between adjacent samples, and F is greater than one when the variance decreases between adjacent samples. Thus, for the Fig. 6 data, the pre-

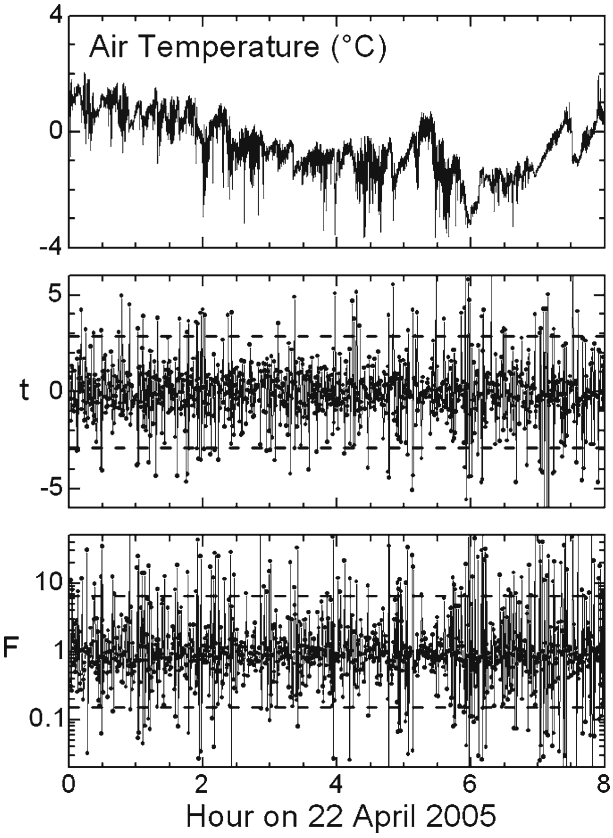

Fig. 6 Air temperature from midnight to 0800 h on 22 April 2005 and corresponding t and F statistics at 30-s intervals. The dashed lines are 99% con dence limits

ferred regime that produces both rst-order and second-order nonstationarity is for the mean to increase while the variance simultaneously decreases.

Such behaviour is evidence of coherent structures, often seen as temperature ramps (Antonia et al. 1979; Phong-anant et al. 1980; Kikuchi and Chiba 1985) in the atmospheric surface layer. Antonia and Chambers (1978), Antonia et al. (1979), Antonia et al. (1982), and Phong-anant et al. (1980) describe such ramps in the unstably strati ed surface layer. Kikuchi and Chiba (1985) and Revelle (1993) report ramps in the stably strati ed surface layer, which is the situation represented in Figs. 6–9. Furthermore, in our case, the ramps seem to be evidence of coherent "sweeps" (e.g., Högström and Bergström 1996) that bring relatively warm air from aloft down to the surface to offset the radiative losses.

While Figs. 6 and 8 suggest that the temperature signal for 0000 to 0800 h on 22 April was nonstationary, our similar analysis shows that temperature is better behaved for 0800 h through midnight. In Fig. 5, the t and F statistics for temperature make fewer excursions outside their 99% con dence bands. During this period, only 2.3% of the t values and only 2.6% of the F values stray outside the 99% con dence bands. These extreme values, however, generally cluster and, thus, indicate isolated nonstationary events within a signal that is basically stationary. In fact, in only 0.3% of the samples from 0800 h through midnight do t and F simultaneously breach their respective 99% con dence limits. Based on this more

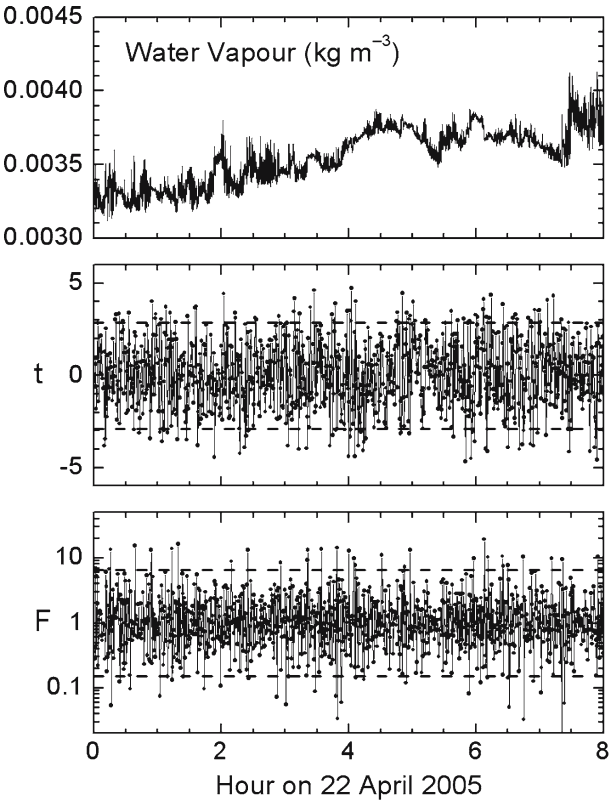

Fig. 7 As in Fig. 6, but this plot is for water vapour density

restrictive definition of nonstationarity, we might conclude that the temperature trace for 0800–2400 h on 22 April in Fig. 3 represents stationary conditions despite the obvious rapid forcing by the clouds.

Figure 9, the scatter plot of t and F for water vapour density for 0000–0800 h on 22 April, contrasts with Fig. 8. Here, 13.6% of the t statistics fall outside the 99% con dence band: that is, they fall in sectors I–IV and b and d. But only 6.3% of the F statistics fall outside the 99% con dence band. Thus, as with Fig. 8, Fig. 9 shows ample evidence of rst-order and second-order nonstationarity. But only a little more than 1% of the samples (10 of 959) in Fig. 9 exhibit rst-order and second-order nonstationarity simultaneously. Consequently, with this more restrictive definition of nonstationarity, we might conclude that the water vapour trace in Fig. 7 is essentially stationary.

Moreover, no samples fall in sector IV, which was the most populated of the simultaneously nonstationary temperature cases in Fig. 8. Only 2 samples fall in sector I either, and only one sample falls in sector II. Thus, in contrast to Fig. 8, 9 of the 10 cases for which t and F are simultaneously outside their 99% con dence bands fall in sector III. Here, both the mean and the variance increase significantly between adjacent samples.

For the other 16 h on 22 April, from 0800 to 2400 h (see Figs. 3 and 5), only 2.1% of the t statistics and only 3.4% of the F statistics for the water vapour density are outside their respective 99% con dence bands. Again, since these are 1% significance tests, we would still

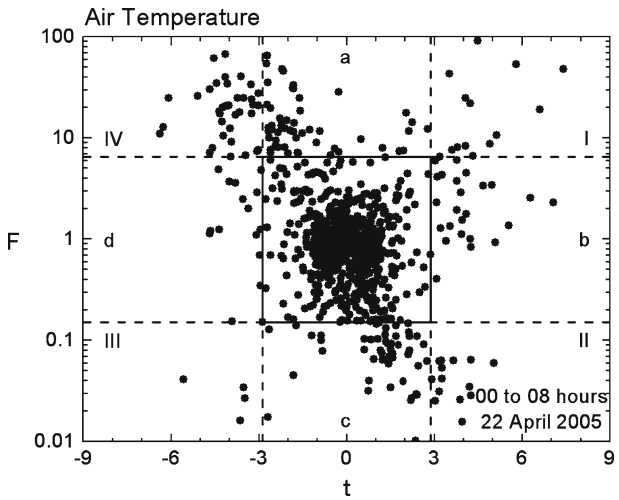

Fig. 8 The t and F statistics for the air temperature data in Fig. 6 are displayed as a scatter plot. Markers within the central box are within both the t and F 99% confidence bands and would indicate stationary data. Markers in sectors a and c indicate first-order stationary but second-order nonstationary data. Markers in sectors b and d indicate first-order nonstationary but second-order stationary data. Markers in sectors I–IV indicate data that are both first-order and second-order nonstationary

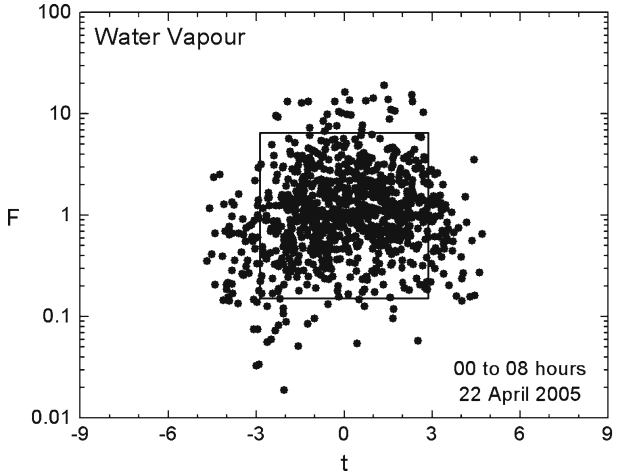

Fig. 9 As in Fig. 8, but this shows the t and F statistics for water vapour density from Fig. 7. This plot would have the same sectors delineated in Fig. 8, but we omit the dashed lines for less cluttered viewing. Markers in the central box indicate strict stationarity

be concerned about nonstationarity in the water vapour signal. But, as with air temperature, the excursions outside the 99% confidence bands for 0800–2400 h, especially for t, occur in clusters. Furthermore, during this 16-h period, in only 0.3% of the total samples do the extremes in t and F occur simultaneously.

5 Conclusions

Our original hypothesis was that changes in cloud forcing immediately affect the surface temperature and, thus, the temperature of the near-surface atmosphere and, perhaps, other near-surface meteorological variables. Our two examples of day-long traces of the radiative forcing and the responses in surface temperature and in near-surface air temperature and humidity (Figs. 2–4) con rm this scenario. The surface temperature responds significantly and typically within a minute to rapid changes in the incoming shortwave and longwave radiation that are associated with changing cloud conditions. The near-surface air temperature quickly follows suit because it is closely coupled to the surface through the sensible heat ux. We also see cases when the near-surface water vapour density also responds to this cloud forcing, presumably through changes in the latent heat ux from the surface or because of changes in boundary-layer mixing.

The second part of our hypothesis was that changes in cloud forcing lead to nonstationarity in the turbulence properties of the near-surface atmosphere. To evaluate this hypothesis, we rst introduced a rigorous definition of nonstationarity. First-order nonstationarity occurs when adjacent means in a time series fail a two-tail t test for equality at the 1% significance level. Second-order nonstationarity occurs when adjacent variances fail a two-tail F test for equality at the 1% significance level. While failing either of these tests is evidence that a time series is nonstationary, an even more restrictive definition of nonstationarity is that a time series must fail both tests before it is identi ed as nonstationary.

We looked for nonstationarity associated with cloud forcing in the air temperature and the water vapour density by introducing new analysis techniques. We rst used the time-dependent memory method (Trevi ño and Andreas 2000) to separate mean and uctuating parts of the air temperature and water vapour signals and to compute corresponding variances. The TDM method is designed specifically to extract means and variances from a signal that is presumed to be nonstationary. With the means and variances from the TDM method, we computed several day-long series of t and F statistics with 30-s spacing. To our knowledge, this is the rst time that t and F statistics have been applied to the problem of identifying rst-order and second-order nonstationarity.

Testing at the 1% significance level, we found in both our examples that the midnight-to-sunrise temperature and water vapour signals were severely nonstationary. Micrometeorologists have known for a long time that nighttime conditions are often nonstationary; our statistics con rm this fact and allow us to assign a probability as to whether a period is stationary or not.

The daylight and early-night data, however, are less conspicuously nonstationary according to our t and F tests, despite examples selected with frequent changes in cloud forcing. We see short clusters of nonstationarity associated with the most extreme changes in cloud forcing. But the rapid, small changes in incoming shortwave radiation in Figs. 3 and 4 that we associated with varying cirrus clouds do not produce severe nonstationarity.

Perhaps Monin–Obukhov similarity functions measured during the day under conditions of variable cloudiness have not been seriously degraded by nonstationarity. On the other hand, our analysis suggests that any similarity functions measured at night over terrestrial surfaces experiencing diurnal forcing likely suffer severely from nonstationarity. Nonstationarity may thus explain the wide range in Monin–Obukhov similarity functions obtained in stable strati cation (e.g., Andreas 2002).

Although here we applied our analysis techniques only to time series, they would work as well for identifying inhomogeneity in spatial series: in data from aircraft turbulence instruments, for example.

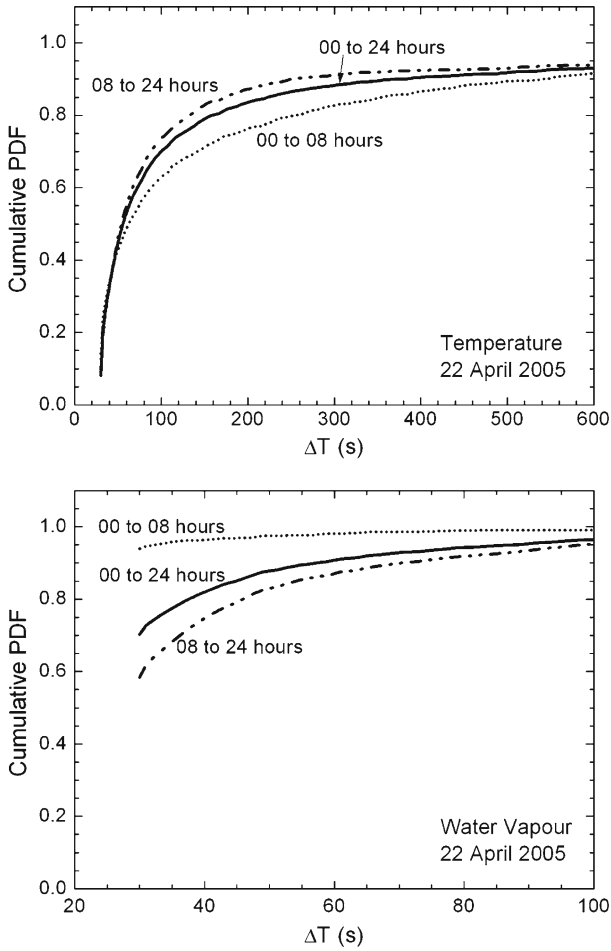

Fig. 10 Cumulative probability density functions for the averaging time ΔT computed for the temperature and water vapour density data collected on 22 April 2005. The three periods identified have different distributions

Acknowledgements We thank three anonymous reviewers and J. R. Garratt for thoughtful comments that helped us improve the manuscript. The U.S. Department of the Army supported this work through Project 611102T2400 at the U.S. Army Cold Regions Research and Engineering Laboratory. We thank Charles C. Ryerson for his early help with this project.

Appendix A: The Averaging Times ΔT and L

To emphasize how the time-dependent memory method differs from standard turbulence averaging, we show here some examples of probability density functions (PDFs) for the two averaging times that the TDM method evaluates. We denote ΔT as the time required to find the mean and as L, referred to as the "memory," the averaging period for finding the variance (or spectrum). Treviño and Andreas (2000) explain how the TDM method finds these times.

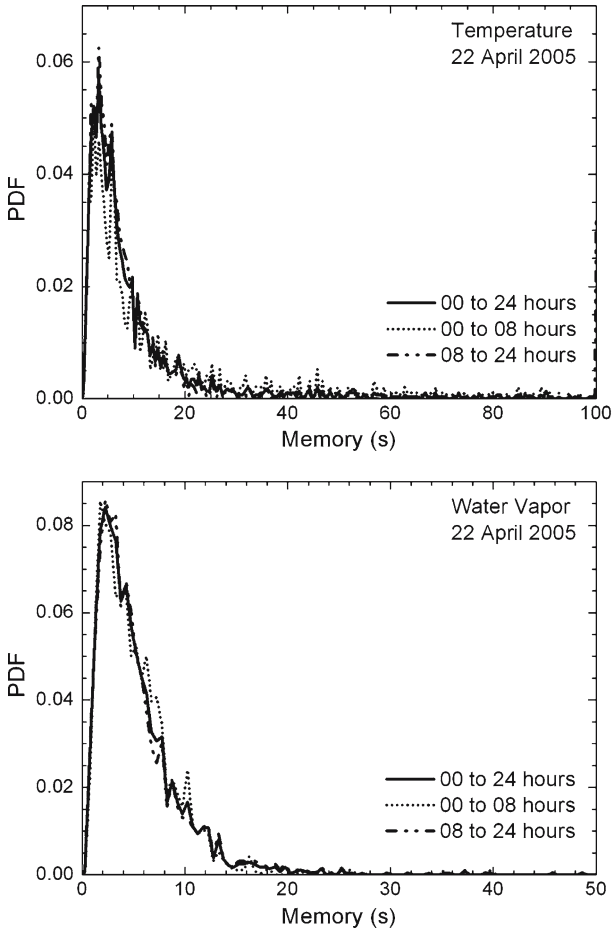

Fig. 11 Probability density functions for the memory, γ, computed for the temperature and water vapour density data from 22 April 2005. As in Fig. 10, the panels show PDFs for three different periods on this day

The majority of the analysis that we reported here concentrated on the temperature and water vapour signals for 22 April 2005 (i.e., Figs. 8–9). Figures 10 and 11 show ΔT and memory values obtained for this day for the same times for which we computed the σ_T and γ_T statistics in Fig. 5.

Figure 10 shows the cumulative probability density functions of ΔT for temperature and water vapour for three periods on 22 April. In our analysis, ΔT was not allowed to be less than 30 s because of the integral scale constraint discussed in Sect. 3. Therefore, all curves in Fig. 10 start at 30 s. A high percentage of our calculations yielded acceptable means with only 30 s of averaging, especially for the water vapour data.

At the other extreme, we did not let ΔT exceed 900 s (i.e., 15 min). A few of our calculations reached this limit without meeting the accuracy constraint that ultimately defines ΔT, as described by Treviño and Andreas (2000). For these few samples, we would say that the TDM method did not converge; but we continued our analysis anyway by using $\Delta T = 900$ s for the sake of having continuous time series of means and variances. In short, the cumulative

PDFs in Fig. 10 do not reach 1.0 at the right edge of the plots because of these values of $\Delta T = 900$ s and a few other unusually large ΔTs that were less than 900 s but greater than the right limits on the horizontal axes in Fig. 10.

Because our discussion in Sect. 4 identified differences in the turbulence signals between the periods midnight to 0800 h and 0800 h to midnight, Fig. 10 shows the cumulative PDFs for these two periods and for the whole day. In each panel in the figure, the trace for the whole day falls between the traces for the early period and for the later period. But the relative positions of the early and later periods switch between the two panels in Fig. 10. That is, for the temperature data, the midnight to 0800 h trace reflects larger ΔT values and thus rises slower than the 0800 h to midnight trace. In the water vapour panel in Fig. 10, the opposite is true. Over 90% of the ΔT values for the midnight to 0800 h period were 30 s, while the 0800 h to midnight period features larger ΔT values.

In summary, from Fig. 10 we conclude that, on this day, 500 s of averaging was sufficient to obtain a meaningful mean for temperature over 90% of the time. Meanwhile, 70 s of averaging was sufficient to evaluate the mean for water vapour density over 90% of the time.

Because we often computed the memory, D, to be less than a second and because, in essence, the memory is the same as the integral scale that we discussed in Sect. 3, we show in Fig. 11 the probability density functions (as opposed to the cumulative PDFs) for the memory for temperature and water vapour on 22 April. Again, Fig. 11 identifies the same three periods as in Fig. 10.

In both panels in Fig. 11, the majority of memory values are smaller than 10 s, and the PDFs peak near 3–6 s for temperature and near 2–4 s for water vapour. These plots therefore corroborate the estimate for the integral scale that we made in Sect. 3 and, in turn, support our decision to calculate t and F statistics every 30 s.

References

Andreas EL (1988) Estimating averaging times for point and path-averaged measurements of turbulence spectra. J Appl Meteorol 27:295–304

Andreas EL (2002) Parameterizing scalar transfer over snow and ice: a review. J Hydrometeorol 3:417–432

Andreas EL, Treviño G (1997) Using wavelets to detect trends. J Atmos Oceanic Technol 14:554–564

Andreas EL, Hill RJ, Gosz JR, Moore DI, Otto WD, Sarma AD (1998) Statistics of surface-layer turbulence over terrain with metre-scale heterogeneity. Boundary-Layer Meteorol 86:379–408

Andreas EL, Fairall CW, Persson POG, Guest PS (2003) Probability distributions for the inner scale and the refractive index structure parameter and their implications for flux averaging. J Appl Meteorol 42:1316–1329

Andreas EL, Geiger CA, Claffey KJ, Treviño G, Ryerson CC (2006) Rapid forcing of the surface and near-surface atmosphere. In: 10th symposium on integrated observing and assimilation systems for the atmosphere, oceans and land surfaces, Atlanta, GA, Amer. Meteorol. Soc., CD-ROM 4.2, 12 pp

Andreas EL, Geiger CA, Treviño G, Claffey KJ (2007) Identifying nonstationarity in the atmospheric surface layer. In: 21st conference on hydrology, San Antonio, TX, Amer. Meteorol. Soc., CD-ROM 5A.8, 12 pp

Antonia RA, Chambers AJ (1978) Note on the temperature ramp structure in the marine surface layer. Boundary-Layer Meteorol 15:347–355

Antonia RA, Chambers AJ, Friehe CA, Van Atta CW (1979) Temperature ramps in the atmospheric surface layer. J Atmos Sci 36:99–108

Antonia RA, Chambers AJ, Bradley EF (1982) Relationships between structure functions and temperature ramps in the atmospheric surface layer. Boundary-Layer Meteorol 23:395–403

Brunk HD (1965) An introduction to mathematical statistics, 2nd edn. Blaisdell, Waltham, Massachusetts, 429 pp

Foken Th, Wichura B (1996) Tools for quality assessment of surface-based flux measurements. Agric Forest Meteorol 78:83–105

Fuehrer PL, Friehe CA (2002) Flux corrections revisited. Boundary-Layer Meteorol 102:415–457

Gao Z, Bian L, Zhou X (2003) Measurements of turbulent transfer in the near-surface layer over a rice paddy in China. J Geophys Res 108(D13):4387, doi:10.1029/2002JD002779
Högström U (1996) Review of some basic characteristics of the atmospheric surface layer. Boundary-Layer Meteorol 78:215–246
Högström U, Bergström H (1996) Organized turbulence structures in the near-neutral atmospheric surface layer. J Atmos Sci 53:2452–2464
Jacobs AFG, Heusinkveld BG, Holtslag AAM (2003) Carbon dioxide and water vapour ux densities over a grassland area in the Netherlands. Int J Climatol 23:1663–1675
Johansson C, Smedman A-S, Högström U, Brasseur JG, Khanna S (2001) Critical test of the validity of Monin–Obukhov similarity during convective conditions. J Atmos Sci 58:1549–1566
Kaimal JC, Finnigan JJ (1994) Atmospheric boundary layers ows: their structure and measurement. Oxford University Press, New York, 289 pp
Kaimal JC, Gaynor JE (1991) Another look at sonic thermometry. Boundary-Layer Meteorol 56:401–410
Kaimal JC, Gaynor JE, Zimmerman HA, Zimmerman GA (1990) Minimizing ow distortion errors in a sonic anemometer. Boundary-Layer Meteorol 53:103–115
Kennel MB (1997) Statistical test for dynamical nonstationarity in observed time-series data. Phys Rev E 56:316–321
Kikuchi T, Chiba O (1985) Step-like uctuations associated with inverted ramps in a stable surface layer. Boundary-Layer Meteorol 31:51–63
Klipp CL, Mahrt L (2004) Flux–gradient relationship, self-correlation and intermittency in the stable boundary layer. Quart J Roy Meteorol Soc 130:2087–2103
Kristensen L, Mann J, Oncley SP, Wyngaard JC (1997) How close is close enough when measuring scalar uxes with displaced sensors? J Atmos Oceanic Technol 14:814–821
Kukharets VP, Tsvang LR (1998) Atmospheric turbulence characteristics over a temperature-inhomogeneous land surface. Part I: statistical characteristics of small-scale spatial inhomogeneities of land surface temperature. Boundary-Layer Meteorol 86:89–101
Lenschow DH, Mann J, Kristensen L (1994) How long is long enough when measuring uxes and other turbulence statistics? J Atmos Oceanic Technol 11:661–673
Lumley JL, Panofsky HA (1964) The structure of atmospheric turbulence. Interscience, New York, 239 pp
Mahrt L (1998) Flux sampling errors for aircraft and towers. J Atmos Oceanic Technol 15:416–429
Pattey E, Strachan IB, Desjardins RJ, Massheder J (2002) Measuring nighttime CO_2 exchange over terrestrial ecosystems using eddy covariance and nocturnal boundary layer methods. Agric Forest Meteorol 113:145–158
Phong-anant D, Antonia RA, Chambers AJ, Rajagopalan S (1980) Features of the organized motion in the atmospheric surface layer. J Geophys Res 85:424–432
Priestley MB (1981) Spectral analysis and time series. Academic Press, San Diego, 890 pp
Revelle DO (1993) Chaos and "bursting" in the planetary boundary layer. J Appl Meteorol 32:1169–1180
Roth M, Oke TR (1995) Relative ef ciencies of turbulent transfer of heat, mass, and momentum over a patchy urban surface. J Atmos Sci 52:1863–1874
Schumann U, Dörnbrack A, Mayer B (2002) Cloud-shadow effects on the structure of the convective boundary layer. Meteorol Z 11:285–294
Siqueira M, Leuning R, Kolle O, Kelliher FM, Katul GG (2003) Modelling sources and sinks of H_2O and heat within a Siberian pine forest using three inverse methods. Quart J Roy Meteorol Soc 129:1373–1393
Sreenivasan KR, Chambers AJ, Antonia RA (1978) Accuracy of moments of velocity and scalar uctuations in the atmospheric surface layer. Boundary-Layer Meteorol 14:341–359
Tennekes H, Lumley JL (1972) A rst course in turbulence. MIT Press, Cambridge, Massachusetts, 300 pp
Treviño G, Andreas EL (2000) Averaging intervals for spectral analysis of nonstationary turbulence. Boundary-Layer Meteorol. 95:231–247
Treviño G, Andreas EL (2006) Dynamical implications of block averaging. Boundary-Layer Meteorol 120:497–508
Vickers D, Mahrt L (1997) Quality control and ux sampling problems for towers and aircraft data. J Atmos Oceanic Technol 14:512–526
Webb EK, Pearman GI, Leuning R (1980) Correction of ux measurements for density effects due to heat and water vapour transfer. Quart J Roy Meteorol Soc 106:85–100
Wilks DS (2006) Statistical methods in the atmospheric sciences, 2nd edn. Academic Press, San Diego, 627 pp
Wyngaard JC (1973) On surface-layer turbulence. In: Haugen DA (ed) Workshop on micrometeorology. American Meteorological Society, Boston, pp 101–149